Journal of Controlled Release 286 (2018) 231–239

Contents lists available at ScienceDirect

Journal of Controlled Release

journal homepage: www.elsevier.com/locate/jconrel

Imaging the porous structure in the core of degrading PLGA microparticles: The effect of molecular weight

Ioanna Mylonaki, Eric Allémann, Florence Delie, Olivier Jordan*

School of Pharmaceutical Sciences, University of Geneva, University of Lausanne, rue Michel Servet 1, CH-1211 Geneva 4, Switzerland

ARTICLE INFO

Keywords:
PLGA microparticles
Pores
Molecular weight
Erosion
Swelling
Drug release mechanism
Atorvastatin

ABSTRACT

The aim of this study was to understand the pore formation mechanisms of degrading poly(D,L-lactic-*co*-glycolic acid) (PLGA) microparticulate systems. This was investigated through an original microparticles cross-section imaging method. Atorvastatin (ATV)-loaded 16- to 18-μm spherical microparticles with polymers of varying molecular weights (8 to 45 kDa) were prepared. The evolution of the particles during *in vitro* drug release experiments was monitored in terms of molecular weight, pore formation and glass transition temperature. During the 2nd phase of release, two types of pores were observed: small pores near the particle's periphery and larger pores in the core. The pattern of pore formation was shown to be related to the shape of the drug release curve. At the onset of the 3rd phase, the polymer transitions to a less glassy state, allowing for the swelling of the microparticles. Overall, we present evidence that pore formation is not uniformly distributed throughout PLGA microparticles, and that it could determine the drug release kinetics.

1. Introduction

Poly(lactic-*co*-glycolic acid) (PLGA)-based drug delivery systems have been widely used to sustain the delivery of a wide variety of active principles, including small hydrophobic molecules, proteins and peptides [1]. However, the drug release mechanisms are still not fully understood. In the quest for a rational selection of microparticle properties (*e.g.* drug loading, size, polymer molecular weight (Mw) [2–6]) that would lead to the targeted release profile [7–9], a better comprehension of the role of these properties is needed.

Up to date, it has been demonstrated that drug release from PLGA microparticles is controlled by three parameters: i) polymer degradation / erosion, ii) polymer swelling and iii) drug transport [10]. Mathematical models have been applied to elucidate how these parameters are transposed to drug release mechanisms [11]. Despite the improvement of these models, their predictive power remains poor [11, 12], especially when triphasic release profiles are observed. This is mainly because two important parameters altering the drug's diffusion path length have until recently not been thoroughly explored: swelling and erosion patterns of the particles. Monitoring of the swelling of microparticles upon exposure to the media has just been achieved by single-particle observation [13, 14]. In these studies, the onset of the third and final phase of triphasic release was related to the swelling phenomena.

In contrast, the erosion pattern has been poorly investigated. Approaches such as Monte Carlo simulations [12] and cellular automaton [15], which attribute uniform stochastic distribution to the erosion pores formed within the particle, fail to predict drug release in a broad range of PLGA microparticulate systems. Instead, it is widely acknowledged that pore formation is more prone to occur in the center of the particle due to autocatalytic phenomena [16]. The occurrence of unevenly distributed pores is likely to modify the release when compared to homogeneous pore distribution. Indeed, it has been acknowledged that the position of the pores affect drug diffusivity within the microparticle spheres [12] and mean path length to microparticle surface.

The aim of the present work is to investigate the evolution of the internal structure of PLGA microparticles during the release of the small hydrophobic model molecule atorvastatin (ATV), in an aqueous medium. As shown in a previously published study, sustained perivascular delivery of atorvastatin using PLGA microspheres could efficiently prevent restenosis in mice [7].

We developed a novel cryosectioning technique to observe systematically the core of the microparticles at several time points during the release study. Cross-sections of freshly prepared, non-degraded particles have previously been published [14, 17, 18]. However, cross-sections of degrading particles are more difficult to obtain as particles become softer and spongy after few days of immersion in an aqueous medium [13, 19–21].

* Corresponding author.
E-mail address: Olivier.Jordan@unige.ch (O. Jordan).

https://doi.org/10.1016/j.jconrel.2018.07.044
Received 17 April 2018; Received in revised form 6 July 2018; Accepted 27 July 2018
Available online 30 July 2018
0168-3659/

For the first time, we present herein micrographs of the evolution of microparticles internal porosity during degradation. As Mw is known to largely influence the erosion profile [22], a comparative study was conducted with polymers of various Mw. The correlation between these observations and the drug release pattern is explored using ATV as a model drug. Glass transition temperature and Mw evolution are also discussed. A scheme linking the microparticles' pore formation and the observed release pattern is proposed.

2. Materials and methods

2.1. Materials

Ester-terminated poly(D,L-lactic-*co*-glycolic acid) (PLGA) with a 50:50 M ratio were used: Resomer® RG502 (i.v. 0.16–0.24 dL/g), RG503 (i.v. 0.32–0.44 dL/g), RG504 (i.v. 0.45–0.60 dL/g) (Evonik Industries AG, Darmstadt, Germany) and RG505 (i.v. 0.61–0.74 dL/g) (Boehringer Ingelheim GmbH, Germany). ATV calcium (βR,δR)-2-(4-Fluorophenyl)-β,δ-dihydroxy-5-(1-methylethyl)-3-(phenyl-d5)-4-[(phenylamino)carbonyl]-1H-pyrrole-1-heptanoic Acid Calcium Salt (2:1) (Chemos GmbH; Regenstauf; Germany), polyvinyl alcohol (PVAL) (Mowiol® 4–88; Kuraray Europe; Hattersheim am Main; Germany), chloroform (Chromasolv® plus for HPLC, ≥ 99.9%, 0.5–1.0% ethanol as stabilizer, Sigma-Aldrich Chemie GmbH; Steinheim; Germany);and Tissue-Tek® O.C.T.™ Compound (Sakura; Alphen aan den Rijn; Netherlands) were used as received. PBS was prepared using monobasic dihydrogen phosphate and dibasic monohydrogen phosphate. All other chemicals were of analytical grade.

2.2. Microparticles preparation and characterization

PLGA 50/50 polymers RG502, RG503, RG504, and RG505 were used. Microparticles were prepared using an oil in water (o/w) emulsion-evaporation process. Briefly, 375 mg of PLGA and 37.5 mg of ATV were dissolved in 7 g of chloroform and emulsified in a PVAL 1% *w/v* aqueous solution at 1500 rpm for 20 min using a paddle stirrer (Eurostar digital, IKA-Werke, Staufen, Germany). The emulsion was added to 50 mL of water and chloroform was evaporated while stirring at 500 rpm overnight. Particles were washed with pure water and concentrated by successive steps of centrifugation/re-suspension before freeze-drying without a cryoprotective agent (Alpha 2–4 LSC, Christ, Kuhner, Switzerland). The supernatant of the final washing step was analyzed for the presence of ATV by direct injection in an HPLC-UV set up to confirm the thorough elimination of non-incorporated drug. The samples were analyzed by reversed phase HPLC (LC module I plus, Waters corporation, Milford, USA), and ATV concentration was assessed with a UV spectrometer set at λ = 245 nm, retention time 7.8 min. The column was a Nucleosil CC 125 / 4120–5 C_{18} (Macherey-Nagel GmbH & Co. KG, Oensingen, Switzerland) maintained at 25 °C. The mobile phase was 55% acetate buffer (10 mM, pH 3) and 45% acetonitrile at a flow rate of 1 mL/min. The calibration curve was prepared by consecutive dilutions of a starting 30% *v*/v ATV ethanolic solution in water (0.781, 1.56, 3.13, 6.25, 12.5, 25.0, 50.0 μg/mL). The curve was constructed using Waters® Millennium®32 Software. The method was fully validated, and a limit of quantification of 500 ng/mL and limit of detection of 50 ng/mL were obtained. A trueness of 98 to 102% was determined, and the intermediate precision was 2%; moreover, the three replicates were injected on three different days to demonstrate the repeatability of the method. The quantification was conducted in triplicate. The results are presented as actual drug loading, corresponding to the percent mass ratio of the encapsulated drug to the mass of the recovered microparticles.

For the drug loading quantification, approximately 4 mg of microparticles were dissolved in 3 mL of acetonitrile. Then, 3 mL of ethanol were added to ensure ATV dissolution. In this case, the calibration curve was prepared in acetonitrile/ethanol. The samples were measured with the HPLC-UV method as described above.

Freeze-dried particles were suspended in water and their size distribution was measured by laser diffraction on a Mastersizer S Long Bench equipped with a small volume sample dispersion unit set at a stirring speed of 1100 rpm (Malvern Instruments Ltd., Worcestershire, UK). The analyses were performed using the Fraunhofer model. The refractive index was set at 1.529 for microparticles and 1.330 for water.

2.3. In vitro ATV release

Briefly, 50 mg of microparticles were immersed in 20 mL of PBS (0.1 M, pH 7.4) / SDS 0.1% and horizontally shaken at 80 rpm in an oven set at 37 °C (EG 110 IR, Jouan, Saint-Herblain, France). At predetermined time intervals, 250 μL aliquots of supernatant were withdrawn and replaced with fresh medium. The samples were analyzed by reversed phase HPLC-UV as described in Section 2.2. The calibration curve was constructed by consecutive dilutions of 30% ATV ethanolic solution in PBS (0.1 M, pH 7.4)/SDS 0.1% (0.781, 1.56, 3.13, 6.25, 12.5, 25.0, 50.0 μg/mL). Each experiment was conducted in triplicate and the values are expressed as the mean ± standard deviation. In identical experimental set ups that were conducted in parallel, 10 mg of microparticles were collected at predetermined time intervals, freeze-dried for 24 h (Alpha 2–4 LSC, Christ, Kuhner, Switzerland) and stored for further analysis (microscopy, differential scanning calorimetry and size exclusion chromatography).

2.4. Scanning electron microscopy imaging

Freeze-dried particles were dispersed in distilled water. Drops of the suspension were placed onto silicon chips glued on electron microscopy stubs, to allow for optimal conductivity. Samples were dried under vacuum, sputter-coated with a 15–20 nm layer of gold and examined by scanning electron microscopy (SEM) using a JSM-7001FA (JEOL, Tokyo, Japan) at 5.0 kV. To obtain cross-sections, particles were embedded in Tissue-Tek® O.C.T.™ Compound (Sakura; Alphen aan den Rijn; Netherlands) and cut in a cryotome (Cryostar™ NX70 Cryostat, Thermo Scientific, Walldorf, Germany). These sections were further sputter-coated and imaged as mentioned above.

2.5. Differential scanning calorimetry

Polymer and freeze-dried microparticle glass transition temperature (Tg) as well as ATV melting point were measured using a Seiko Instruments SSC/5200 SII DSC220C differential scanning calorimeter system with cooling controller. A preparation cycle of heating and cooling back from −30 °C to 200 °C was used to eliminate polymer thermal history. After that, measurements were taken from −30 °C to 200 °C, at a heating rate of 10 °C/min and a hold time of 2 min. Tg was determined during the 2nd heating cycle and calculated as the intersection of the two tangents at the start of the corresponding endotherm of the heat flow curve using the software Origin Pro 8. ATV melting point was measured at the 1st heating cycle at the apex of the peak.

2.6. Size exclusion chromatography

Polymers and freeze-dried microparticles were submitted to gel permeation chromatography in triplicate after freeze-drying. Samples of 10 mg were dissolved in dry THF and then filtered with a Durapore 0.45-μm filter. Measurements were performed using a Waters 515 HPLC pump and a Waters HPLC 717 plus autosampler coupled to a series of Styragel 7.8 × 300 mm columns (HR1 to 4 THF, Waters, Ireland). Samples were monitored using a refractive index detector (Waters 2414, Waters). The calibration curve was constructed using a Waters® Millennium®32 Software with a polystyrene PSS standards polymer kit (Polymer Standards Services GmbH, Mainz, Germany). The mobile phase was THF flowing at a rate of 1 mL/min, the run time was 45 min and the injection volume 200 μL. All Mw are presented as weight-average Mw.

Table 1
Physicochemical properties of the microparticles formulated with polymers of different Mw. 10% -> 1%?

Microparticles	Mw[a] (kDa)	Lactic:glycolic ratio	D(4,3), span (μm)	ATV loading (*w*/w) (%)
M502	8	50:50	16, 1.962	1.6 ± 0.5
M503	32	50:50	17, 1.883	1.0 ± 0.4
M504	37	50:50	18, 1.484	1.2 ± 0.2
M505	45	50:50	18, 2.001	1.2 ± 0.4

[a] Mw determined after formulation as microparticles.

3. Results

3.1. Microparticles characterization

Initially, microparticle fabrication parameters such as polymer lactic/glycolic ratio, polymer Mw, organic/aqueous phase ratio, stirring speed, salts addition and use of co-solvents, were investigated (Table S.I.1). We then focused on four types of microparticles, prepared from polymers of different Mw (18 kDa, 39 kDa, 45 kDa and 50 kDa as determined by size-exclusion chromatography). The Mw of the microparticles obtained with these polymers (M502, M503, M504 and M505, respectively) are presented in Table 1. The ATV loading and the average microparticle diameters were similar for all Mw, although the size distributions were not monodispersed.

3.2. In vitro drug release profile

Fig. 1A shows the release profile of ATV from the microparticles prepared from polymers with different Mw. For M502, M503 and M504 a substantial burst release of 28%, 12% and 5% was observed, respectively, over the first 8 h. The initial release for M505 was < 1%. For M502, the drug release was led by a diffusion process, as supported by fitting with a first-order release kinetics curve [23] (data not shown, $R^2 = 0.98$). In contrast, the M503, M504 and M505 demonstrated triphasic curves. For these polymers, following the burst release within the first 8 h, a 2nd phase was observed up to day 17. The 3rd phase from day 20 to day 35 was characterized by an increased release rate, compared to the 2nd phase.

In Fig. 1B, the correlation between the initial Mw of the microparticles and the ATV release profile is explored. The different phases of the drug release were investigated separately. The amount released during the burst phase was shown to linearly correlate to the Mw (Fig. 1 B1). For the 2nd phase (8 h to day 17) a linear correlation was observed between the Mw and the mean 2nd-phase release rate, expressed as the slope of the curve (Fig. 1 B2). The 3rd phase release profile (M503, M504, and M505) was independent of the Mw, as all curves had the same slope (Fig. 1 B3). The release duration, defined as the time needed for the release curve to reach the final plateau ± 5%, was similar for all microparticles (approx. 37 days), except M502 (23 days) (Fig. 1 B4). As the release profiles from M504 and M505 were analogous, only the release profile of M504 was further characterized.

3.3. Differential scanning calorimetry

ATV melting point was measured to be 159.3 °C. The evolution of the Tg of the microparticles at different time points of incubation is shown in Fig. 2. ATV-loaded microparticles had a Tg of 39.0 °C - 43.1 °C before the *in vitro* drug release trials. The Tg of the polymers significantly decreased after a few days, shifting the systems to a less glassy state. This occurred between day 6 and 9 for M502 and later for M503 and M504: between day 12 and day 16, respectively.

3.4. Imaging microparticles degradation

SEM micrographs representative of M502, M503 and M504 microparticles degradation over 28 days of *in vitro* release are presented in Fig. 3. Particles were imaged after separation from the dispersing aqueous medium and desiccation. The surface of the particles were smooth and slick before incubation in PBS/SDS 0.1% (Fig. 3, day 0). The surface of the M502 particles showed signs of corrugation already at day 5, evolving progressively up to day 20, when particles presented inward folding. At day 28, particles appeared as “deflated balls.” In contrast, the surface of M503 and M504 particles remained smooth until day 16, and the first signs of corrugation were seen at day 20. Folding appeared after day 24. The smaller the particles, the faster the steps described above progressed. As the particles were dried for SEM observation, the changes of the surface of degrading microparticles suggest a swollen state when dispersed in the release medium. Finally, the craters frequently observed at the surface of the particles (*e.g.*, Fig. 3, M504 day 10 and 16) are likely artifacts due to the abrupt detachment of particles that were previously attached. These artifacts provide information on the pore formation near the periphery (up to 1 μm inward from the surface of the particle).

In Fig. 4 cross-sectioned particles of similar diameters demonstrated the degradation process of the core over time. During incubation, two categories of macropores (according to IUPAC definition [24]) were formed: the small ones (~100 nm) near the periphery and the large ones (~1 μm) observed in the core of the particle. For M502, small pores were observed near the surface of the particles after 5 days of incubation. At day 10, the peripheral porosity increased, while bigger pores appeared within the core of the particle. After 16 days, the pores of the core increased in size, and some peripheral pores were open at the surface due to erosion.

In contrast, for M503 and M504 microparticles at day 5, small pores formed in the core of the particle, which progressively grew in size, up to day 10. At day 16, small size peripheral porosity appeared (Fig. 3), as revealed by the crater-like openings on microparticle surface arising from abrupt detachment of particles. Peripheral porosity was confirmed when observing cross-sections (Fig. 4). Between day 16 and day 20 generalized pore formation was noted within the polymer matrix near the periphery and the core. After day 20, particles swelled significantly precluding cross-sectioning with our technique, as microparticles collapsed upon drying (Fig. 3). This supports extensive swelling of particles after day 20.

3.5. Mw decrease

Size exclusion chromatography was employed to monitor the evolution of polymer Mw during 30 days of incubation of M502, M503 and M504 (Fig. 5). The Mw of M502 decreased by 50% over the 30 days of incubation. Instead, high Mw M503, M504 decreased by 60 to 80% during the same period. The curve was linear for all polymers.

4. Discussion

A better understanding of the influence of PLGA microparticle's characteristics on their drug release kinetics is needed. In the present study, we attempted to gain novel insight on the mechanisms of drug release by investigating the pore formation pattern inside the particle matrix. The drug release is influenced by several parameters among

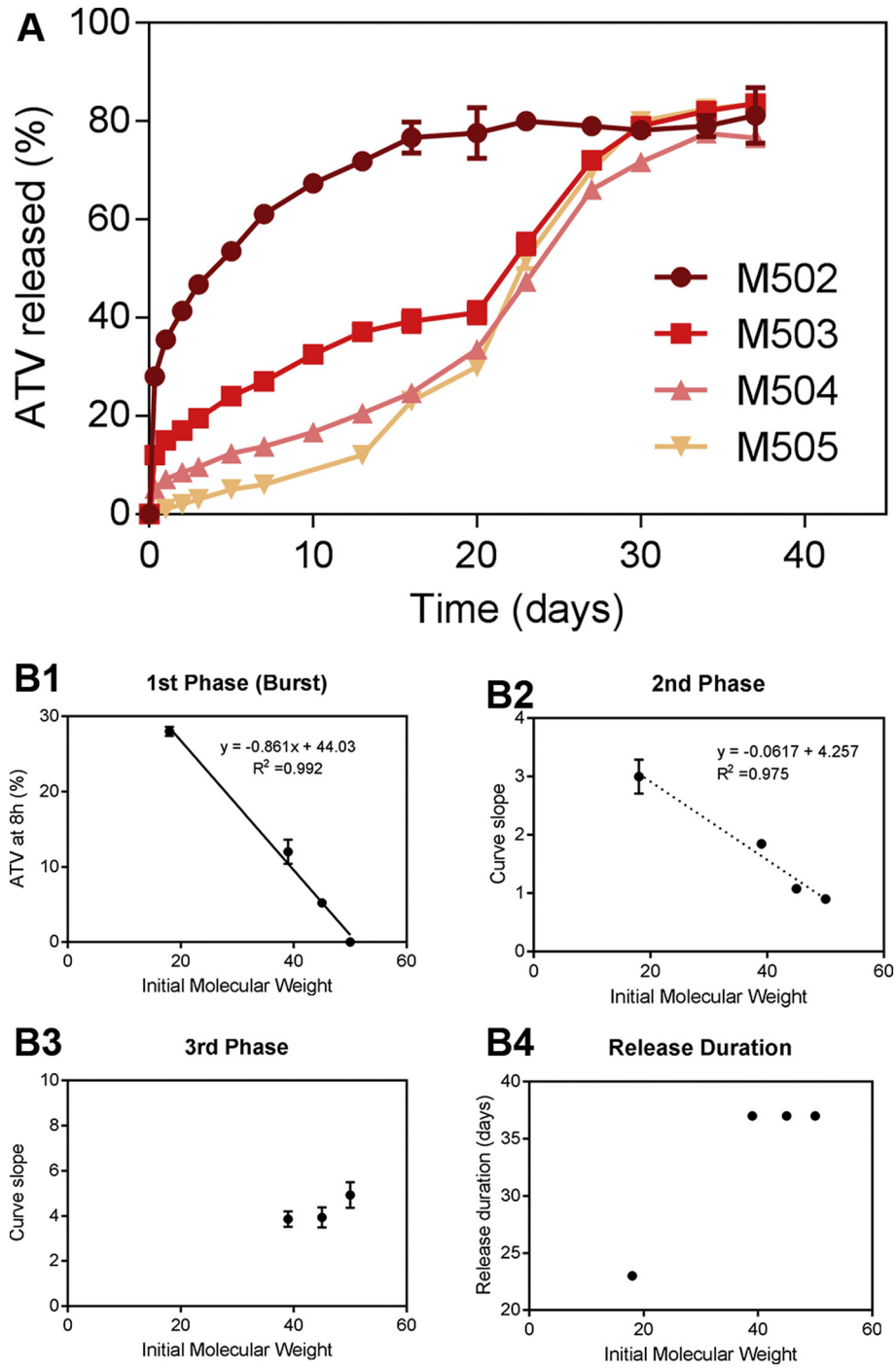

Fig. 1. A: Cumulative ATV release from M502, M503, M504 and M505 microparticles *in vitro* (PBS (0.1 M, pH 7.4)/SDS 0.1%). Each point is a mean ± SD (n = 3). B: Correlations between polymers' initial Mw and the different phases of release. Correlation with B1: percentage of total ATV released during the burst phase (1st phase) after 8 h of incubation, B2: slope of the linear fit during the 2nd phase of ATV release (day 1 to day 17), B3: slope of the linear fit during the 3rd phase of ATV release (day 20 to day 30) only for the 3 types of microparticles displaying this phase and B4: release duration in days for the 4 types of microparticles.

which are: particle diameter, polymer type (copolymer ratio, crystallinity, Mw), polymer/drug interaction, and diffusion coefficient of the drug [25–27]. We focused on the influence of the Mw parameter, known to play a key role in release kinetics [22, 28]. To this aim, we generated ATV-loaded PLGA microparticles of different Mw, using an oil/water emulsification process. Diameter, copolymer ratio and drug loading were set at fixed values, to enable comparison of pore formation patterns between the different batches of microparticles.

The low Mw, M502 (Fig. 1), gave a typical diffusion-driven release curve, while triphasic ATV release profiles were observed for high Mw polymers. Makino et al. also showed a shift towards the triphasic release of estradiol for higher Mw PLGA microparticles containing 75% lactide monomer [29]. Raman et al. obtained similar kinetic trends for piroxicam released from 10- and 50-μm PLGA (50% lactide ratio) microparticles of various Mw [28]. The similarities of these results, despite the differences in the physicochemical properties of the molecules (ATV: logP 5, water solubility: 1.23 mg/mL, Mw: 559 g/mol; estradiol: logP 3.57, water solubility: 0.0213 mg/mL, Mw: 272 g/mol and piroxicam: logP 0.6–2.2, water solubility: 0.143 mg/mL, Mw: 331 g/mol support that the Mw of the polymer is indeed a critical parameter

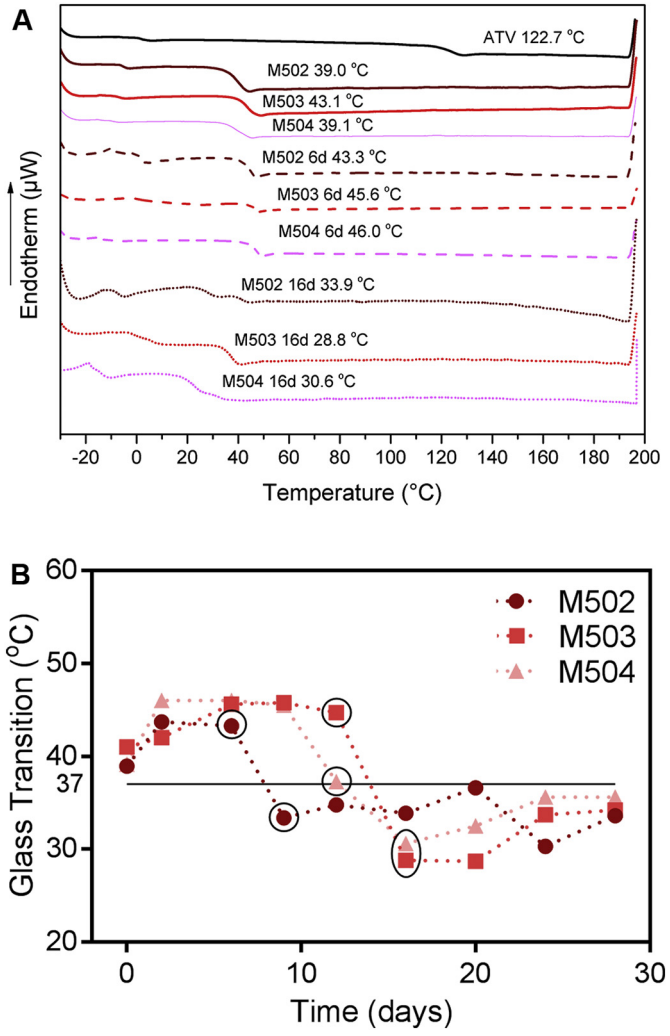

Fig. 2. A: Thermograms of ATV (with melting point value) and ATV-loaded microparticles M502, M503, and M504 (with Tg values) after 0, 6 and 16 days of incubation. B: Evolution of Tg of the ATV-loaded microparticles during the 28 days of the drug release assay. Circles indicate a significant shift of the glass transition temperature.

governing the shape of the release curve.

4.1. Burst release – initial Mw dependence

The extent of the burst release, occurring during the first 8 h of incubation, was suppressed as the Mw of microparticles increased (Fig. 1). In fact, for M505, no burst release was observed. The burst is commonly attributed to non-encapsulated drug detaching from the surface and being dissolved rapidly in the medium [30]. However, this mechanism has been questioned [31]. In our case, microparticles were thoroughly rinsed after preparation until no ATV could be detected in the supernatant. Moreover, we did not observe non-encapsulated ATV attached to the surface of the microparticles in the form of crystals, on the SEM images (Fig. 3). As the mean diameter and drug loading are similar for all microparticles, the diffusion coefficient would only depend on the polymer's Mw (Fig. 1 B1) [32]. Our observations are consistent with a burst phase directly linked to a decrease of diffusion coefficient of the drug through the matrix [33]. The shorter polymer chains allow easier water penetration that could then carry out the dissolved drug by diffusion. Interestingly, our data show the diffusion coefficient of this step of the release process is related to the polymer's initial Mw.

4.2. Second phase of the release – pore formation

4.2.1. Pore formation during 2nd phase of release

The 2nd phase of the drug release (day 5 to day 20, Fig. 1A) is probably the most complex and the least investigated phase of triphasic drug release profiles. In Fig. 1 B2, a negative pseudo-correlation is observed between the microparticles' initial Mw and the ATV mean release rate. During the 2nd phase, the sections of degrading microparticles, demonstrated the growth of a complex pattern of closed pores appearing in the matrix of the particles (Fig. 4). Because the pores are not interconnected to form channels opened to the surface, the release mechanism of the small Mw hydrophobic ATV is still related to the conventional diffusion through the polymeric network [10, 23, 34]. However, since the polymer matrix is disrupted by the appearance of pores we hypothesize that the pattern of pore formation could also be an important parameter influencing the release of ATV molecules out of the particle.

4.2.2. Influence of Mw on pattern of pore formation

Interestingly, we observe that depending on the Mw of the particles, pore patterns vary in location, size, number and time of formation (Figs. 4, 5). Indeed, large (~1 μm) pores are formed in the core of the M503 and M504 particles until day 16, when the Mw is higher than 20 kDa. Instead, the formation of small (~100 nm) pores is observed on low Mw microparticles (M502 already at day 5), or when M503 and M504 microparticles Mw falls below 20 kDa, after day 16 (Fig. 2). The explanation for the mechanism underlying these observations is given below.

4.2.3. Pore formation pattern relates to acidic byproduct concentration

The pore formation is commonly attributed to the acidic conditions that develop in the particle due to polymer hydrolysis, generating an autocatalytic process [16, 35]. For pores developing in the microparticle's core, the autocatalytic phenomenon has been described to occur at the center of the particles where the diffusion pathways are long and acidic by-products are trapped in the matrix [11, 16]. In the present study, it is shown that pores also develop close to the periphery (Fig. 4), albeit smaller in size compared to inner pores. We suggest that the presence of these pores implies autocatalytic phenomena occurring near the periphery of the particles. Due to their location close to the edge of the matrix, the acidic byproducts would be rapidly cleared by diffusion, and the concentration is likely to be lower than in the core pores, thus limiting outer pores growth in size.

4.2.4. Influence of pore formation on drug release

The pore formation could impact the 2nd phase of the release. These pores would be saturated in oligomeric fractions of the polymer chain and ATV in solution in the release medium. At the end of the 2nd phase of the release profile, the ATV molecules would hardly diffuse through the less rubbery (lower Tg) polymeric matrix, explaining the lag-phase plateau reached at the end of the 2nd phase. This mechanism is schematized in Fig. 6.

Overall, we bring new evidence showing that the pore formation in microparticle matrices is not homogenously distributed in the particles as admitted when Monte Carlo simulations or cellular automaton are used for mathematical modeling of drug release [12]. Our results also suggest that the pore formation could have an important impact on the shape of the 2nd phase of the triphasic release profile curve.

4.3. Third phase of the release – swelling

4.3.1. The 3rd phase coincides with the onset and progression of particle swelling

The 3rd phase of the release (from day 20 on) was shown to be independent of the initial Mw of the microparticles, as all curves escalated quickly to the end of the release (Fig. 1 B3). Folded and

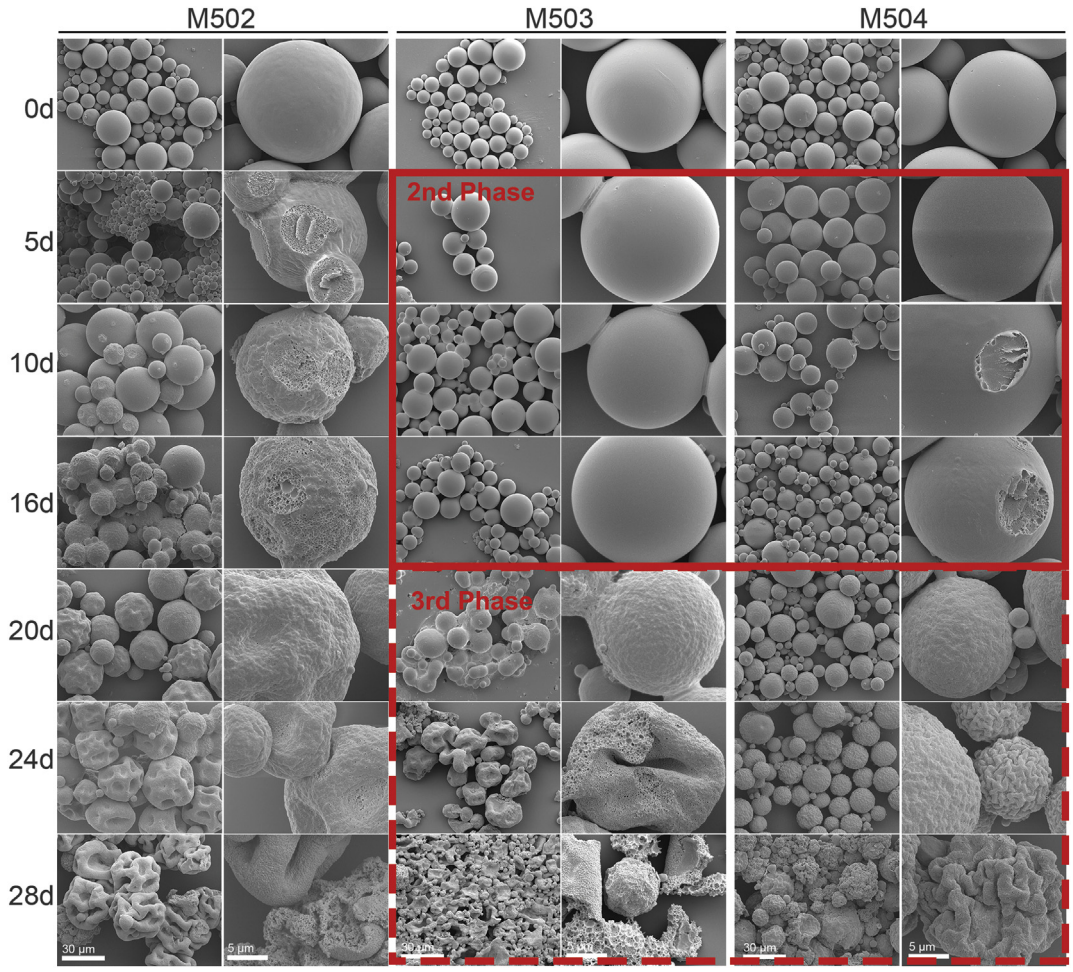

Fig. 3. High and low magnification (scale at 30 and 5 µm, respectively) SEM microphotographs of M502, M503 and M504 microparticles after incubation in PBS (0.1 M, pH 7.4)/SDS 0.1% for up to 28 days. The 2nd and 3rd release phases are highlighted.

collapsed microparticles appeared on the SEM images of dried M503 and M504 at the end of the 2nd phase, typically arising from the drying of microparticles that swelled during incubation. Similar swelling-induced surface wrinkles and corrugation were observed when 0.3%-loaded estradiol was released from other PLGA 75/25 microparticles [29].

4.3.2. Swelling is driven by osmotic pressure

As described by Gu et al., swelling is due to osmotic phenomena [20]. Microparticle swelling has been shown to play a decisive role in the 3rd phase of drug release kinetics [13, 20]. In our case, as the pores are likely saturated with ATV as well as PLGA oligomers, the osmotic pressure gradient triggers water penetration. Once swelling is established, the drug diffusion will accelerate due to enhanced water transport. In a study monitoring the swelling of PLGA microparticles, the onset of the 3rd phase of the release coincided with the swelling onset [13].

4.3.3. Pore formation and swelling

In this study we show that the degree of pore formation has to be considered as a critical parameter for the extent of swelling. For M502, signs of surface collapse upon drying appeared earlier, during the 2nd phase from day 10 on, and corrugation already at day 5 suggesting an early water intake. Thus M502 rapidly swells, while for M503 and M504 the swelling occurs after day 20. In a qualitative visual evaluation of the microparticles cross-sections, we observed that for M502, total cavity area was significantly higher compared to M503 and M504 (Fig. 4). We propose that the volume of pores defines the extent of the swelling and subsequently the drug release kinetics.

4.3.4. Tg/Mw relates to swelling

Additionally, our data for M503 and M504 show that the onset of the swelling (Fig. 3) associates with a shift of the polymer glass transition temperature (Fig. 2). In contrast, M502 swelling initiated earlier, concomitant with an earlier Tg shift, as the smaller initial length of the polymeric chains allowed the swelling of the polymeric matrix. Indeed, another a factor affecting microparticles swelling is the progressive shortening of polymer chain length. It has been suggested that a polymer Mw below 20 kDa is necessary for the initiation of the swelling [13], which is supported by our observations (Figs. 2 and 3). Overall, our results suggest that the microparticle swelling (3rd release phase) is associated with a Tg shift and Mw decay below a critical threshold [14].

Fig. 6 summarizes the time evolution of the microparticles' inner structure that triggers the ATV release, as supported by our results. The 1st phase (burst) is the release of ATV by diffusion from the periphery of the particles. During the 2nd phase, polymer cleavage progresses and elicits the creation of peripheral and core pores. An equilibrium of ATV released and/or trapped in the pores could explain the lag phase observed at the end of the 2nd phase. At the onset of the 3rd phase, the Mw drops below 20 kDa and the polymer glass transition temperature drops significantly, allowing microparticle swelling. The swelling generates osmotic pressure that enhances the diffusion-driven release of ATV.

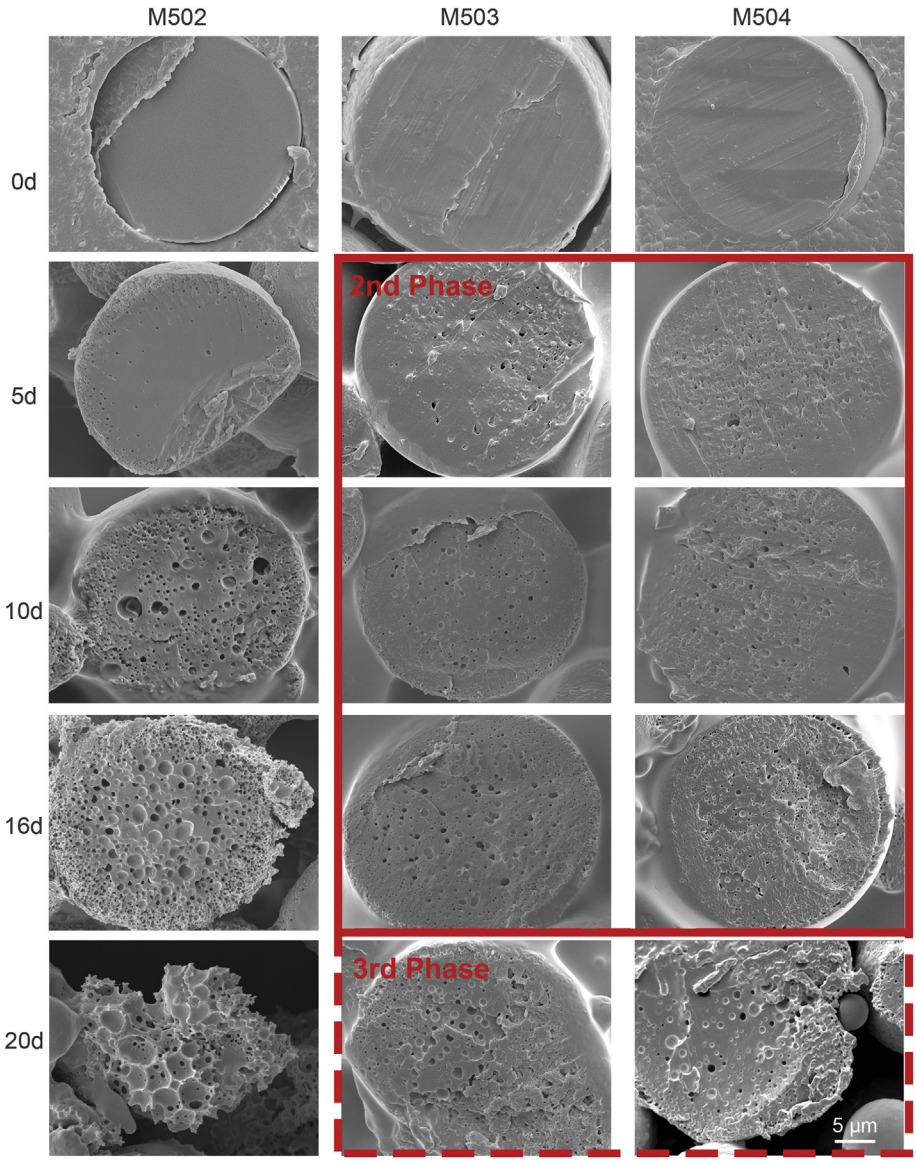

Fig. 4. High magnification (scale at 5 µm) SEM micrographs of M502, M503 and M504 microparticle cross-sections after incubation in PBS (0.1 M, pH 7.4)/SDS 0.1% for up to 20 days. The 2nd and 3rd release phases are highlighted.

5. Conclusion

In this study, we attempted to gain further insight on how drug release profile is influenced by the evolution of microparticles' inner microstructure and polymer physical state. Over the release period, two well-defined pore populations grew within the microparticles. The pore formation pattern was shown to be directly related to the Mw and/or glass transition temperature of the polymer. Small peripheral pores were formed when the Mw was < 20 kDa whereas larger core pores were observed above this Mw value. Mw decay below this threshold

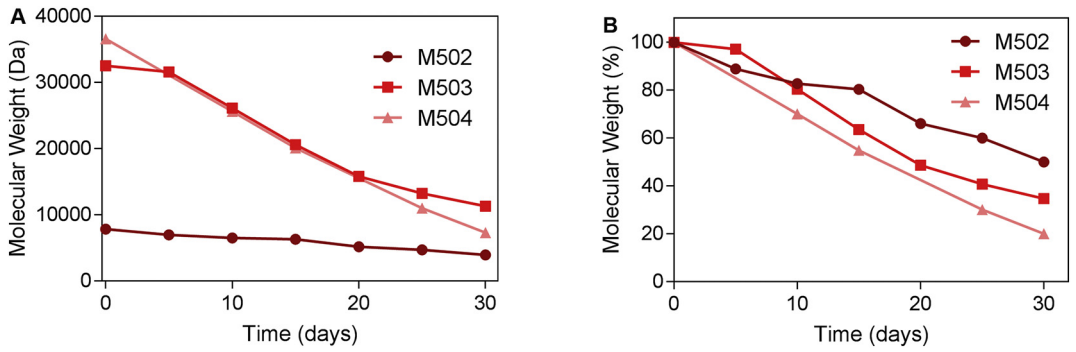

Fig. 5. Evolution of the Mw of M502, M503, M504 particles during incubation in PBS (0.1 M, pH 7.4)/SDS 0.1%.

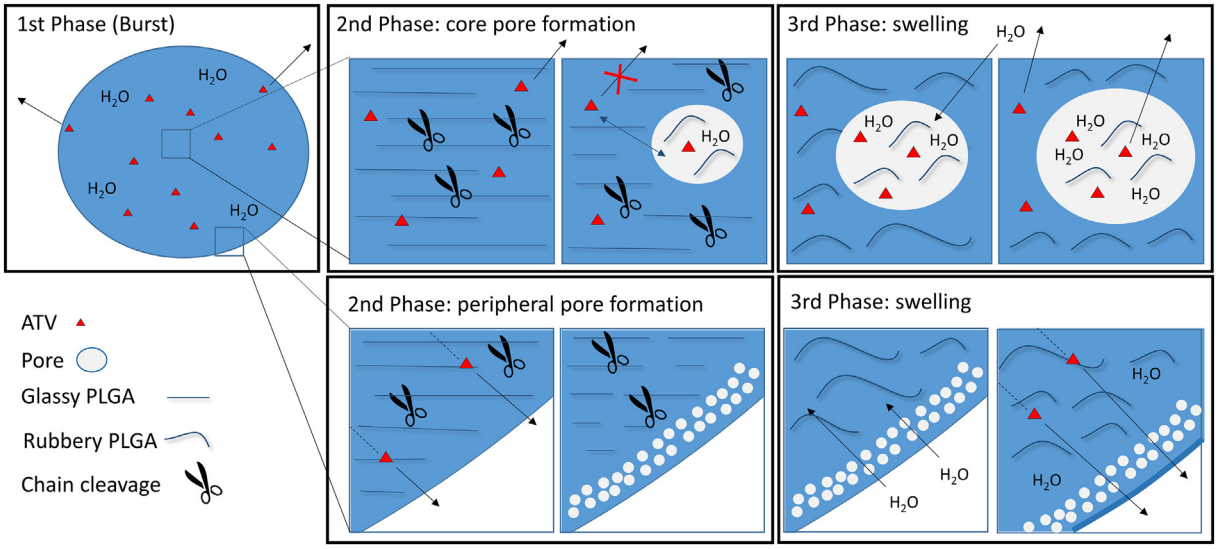

Fig. 6. Schematic representation of a degrading ATV-loaded microparticle showing a large core and small peripheral pore formation during the different phases of drug release. Burst phase: No porosity. 2nd phase: Pores develop due to acidic by-product accumulation. 3rd phase: The existing pores, saturated in ATV and PLGA oligomers, trigger the particle swelling.

associated with a significant Tg decrease towards a more rubbery material. In correlation with the drug release profile, we suggest that the formation of large core pores could enable drug sequestration and prevent its release. Once the polymer Mw drops below the threshold and the glass transition temperature decays, swelling is favored, and the osmotic phenomena encourage the release of ATV. The pattern of pore formation is thus likely to play a critical role in modulating the drug release profile. The non-homogeneous pore distribution warrants the refinement of mathematical models towards more accurate predictions. These results shed light on the importance of the microparticles' internal microstructure evolution, bringing forward the importance of the development of refined imaging techniques to understand the kinetics of drug release from biodegradable microparticles.

Acknowledgements

The authors thank Mrs. Nathalie Boulens for her contribution to the observation of the SEM samples.

Appendix A. Supplementary data

Supplementary data to this article can be found online at https://doi.org/10.1016/j.jconrel.2018.07.044.

References

[1] Y. Zhang, H.F. Chan, K.W. Leong, Advanced materials and processing for drug delivery: the past and the future, Adv. Drug Deliv. Rev. 65 (2013) 104–120.
[2] U. Bilati, E. Allemann, E. Doelker, Poly(D,L-lactide-co-glycolide) protein-loaded nanoparticles prepared by the double emulsion method-processing and formulation issues for enhanced entrapment efficiency, J. Microencapsul. 22 (2005) 205–214.
[3] U. Bilati, E. Allemann, E. Doelker, Development of a nanoprecipitation method intended for the entrapment of hydrophilic drugs into nanoparticles, Eur. J. Pharm. Sci. 24 (2005) 67–75.
[4] J.C. Leroux, E. Allemann, E. Doelker, R. Gurny, New approach for the preparation of nanoparticles by an emulsification-diffusion method, Eur. J. Pharm. Biopharm. 41 (1995) 14–18.
[5] M.J. Blanco-Prieto, E. Leo, F. Delie, A. Gulik, P. Couvreur, E. Fattal, Study of the influence of several stabilizing agents on the entrapment and in vitro release of pBC 264 from poly(lactide-co-glycolide) microspheres prepared by a w/o/w solvent evaporation method, Pharm. Res. 13 (1996) 1127–1129.
[6] N. Butoescu, O. Jordan, A. Petri-Fink, H. Hofmann, E. Doelker, Co-encapsulation of dexamethasone 21-acetate and SPIONs into biodegradable polymeric microparticles designed for intra-articular delivery, J. Microencapsul. 25 (2008) 339–350.
[7] I. Mylonaki, F. Strano, S. Deglise, E. Allémann, F. Alonso, J.-M. Corpataux, C. Dubuis, J.-A. Haefliger, O. Jordan, F. Saucy, F. Delie, Perivascular sustained release of atorvastatin from a hydrogel-microparticle delivery system decreases intimal hyperplasia, J. Control. Release 232 (2016) 93–102.
[8] M. Gaumet, R. Gurny, F. Delie, Fluorescent biodegradable PLGA particles with narrow size distributions: preparation by means of selective centrifugation, Int. J. Pharm. 342 (2007) 222–230.
[9] M.J. Blanco-Prieto, F. Delie, E. Fattal, A. Tartar, F. Puisieux, A. Gulik, P. Couvreur, Characterization of V3 BRU peptide-loaded small PLGA microspheres prepared by a (w1/o)w2 emulsion solvent evaporation method, Int. J. Pharm. 111 (1994) 137–145.
[10] S. Fredenberg, M. Wahlgren, M. Reslow, A. Axelsson, The mechanisms of drug release in poly(lactic-co-glycolic acid)-based drug delivery systems—a review, Int. J. Pharm. 415 (2011) 34–52.
[11] J. Siepmann, F. Siepmann, Mathematical modeling of drug delivery, Int. J. Pharm. 364 (2008) 328–343.
[12] J. Siepmann, N. Faisant, J.-P. Benoit, A new mathematical model quantifying drug release from bioerodible microparticles using Monte Carlo simulations, Pharm. Res. 19 (2002) 1885–1893.
[13] H. Gasmi, F. Danede, J. Siepmann, F. Siepmann, Does PLGA microparticle swelling control drug release? New insight based on single particle swelling studies, J. Control. Release 213 (2015) 120–127.
[14] H. Gasmi, J.F. Willart, F. Danede, M.C. Hamoudi, J. Siepmann, F. Siepmann, Importance of PLGA microparticle swelling for the control of prilocaine release, J. Drug Deliv. Sci. Tec. Part A (2015) 123–132.
[15] N. Bertrand, G. Leclair, P. Hildgen, Modeling drug release from bioerodible microspheres using a cellular automaton, Int. J. Pharm. 343 (2007) 196–207.
[16] L. Li, S.P. Schwendeman, Mapping neutral microclimate pH in PLGA microspheres, J. Control. Release 101 (2005) 163–173.
[17] D. Klose, F. Siepmann, K. Elkharraz, J. Siepmann, PLGA-based drug delivery systems: importance of the type of drug and device geometry, Int. J. Pharm. 354 (2008) 95–103.
[18] D. Klose, F. Siepmann, K. Elkharraz, S. Krenzlin, J. Siepmann, How porosity and size affect the drug release mechanisms from PLGA-based microparticles, Int. J. Pharm. 314 (2006) 198–206.
[19] J. Siepmann, K. Elkharraz, F. Siepmann, D. Klose, How autocatalysis accelerates drug release from PLGA-based microparticles: a quantitative treatment, Biomacromolecules 6 (2005) 2312–2319.
[20] B. Gu, X. Sun, F. Papadimitrakopoulos, D.J. Burgess, Seeing is believing, PLGA microsphere degradation revealed in PLGA microsphere/PVA hydrogel composites, J. Control. Release 228 (2016) 170–178.
[21] X. Luan, R. Bodmeier, Modification of the tri-phasic drug release pattern of leuprolide acetate-loaded poly(lactide-co-glycolide) microparticles, Eur. J. Pharm. Biopharm. 63 (2006) 205–214.
[22] T.G. Park, Degradation of poly(d,l-lactic acid) microspheres: effect of molecular weight, J. Control. Release 30 (1994) 161–173.
[23] J. Siepmann, F. Siepmann, Modeling of diffusion controlled drug delivery, J. Control. Release 161 (2012) 351–362.
[24] B.D. Zdravkov, J.J. Čermák, M. Šefara, J. Janků, Pore classification in the characterization of porous materials: a perspective, Cent. Eur. J. Chem. 5 (2007) 385–395.
[25] C. Berkland, K. Kim, D.W. Pack, PLG microsphere size controls drug release rate through several competing factors, Pharm. Res. 20 (2003) 1055–1062.
[26] J. Siepmann, N. Faisant, J. Akiki, J. Richard, J.P. Benoit, Effect of the size of biodegradable microparticles on drug release: experiment and theory, J. Control. Release 96 (2004) 123–134.

[27] F. Alexis, S.K. Rath, S.S. Venkatraman, Controlled release from bioerodible polymers: effect of drug type and polymer composition, J. Control. Release 102 (2005) 333–344.
[28] C. Raman, C. Berkland, K. Kim, D.W. Pack, Modeling small-molecule release from PLG microspheres: effects of polymer degradation and nonuniform drug distribution, J. Control. Release 103 (2005) 149–158.
[29] K. Makino, T. Mogi, N. Ohtake, M. Yoshida, S. Ando, T. Nakajima, H. Ohshima, Pulsatile drug release from poly (lactide-co-glycolide) microspheres: how does the composition of the polymer matrices affect the time interval between the initial burst and the pulsatile release of drugs? Colloids Surf. B 19 (2000) 173–179.
[30] F. Alexis, S. Kumar Rath, F. Boey, S. Venkatraman, Study of the initial stages of drug release from a degradable matrix of poly(D,L-lactide-co-glycolide), Biomaterials 25 (2004) 813–821.
[31] S.N. Rothstein, W.J. Federspiel, S.R. Little, A simple model framework for the prediction of controlled release from bulk eroding polymer matrices, J. Mater. Chem. 18 (2008) 1873–1880.
[32] S.D. Allison, Analysis of initial burst in PLGA microparticles, Expert Opin. Drug Deliv. 5 (2008) 615–628.
[33] K.M. Gallagher, O.I. Corrigan, Mechanistic aspects of the release of levamisole hydrochloride from biodegradable polymers, J. Control. Release 69 (2000) 261–272.
[34] C. Busatto, J. Pesoa, I. Helbling, J. Luna, D. Estenoz, Effect of particle size, polydispersity and polymer degradation on progesterone release from PLGA microparticles: experimental and mathematical modeling, Int. J. Pharm. 536 (2018) 360–369.
[35] Y. Liu, S.P. Schwendeman, Mapping microclimate pH distribution inside protein-encapsulated PLGA microspheres using confocal laser scanning microscopy, Mol. Pharm. 9 (2012) 1342–1350.